# Quantum-optical nature of the recollision process in high-order-harmonic generation

I. K. Kominis,[1] G. Kolliopoulos,[1,2] D. Charalambidis,[3] and P. Tzallas[2,*]
[1]*Department of Physics, University of Crete, 71103 Heraklion, Greece*
[2]*Foundation for Research and Technology—Hellas, Institute of Electronic Structure & Laser, 71110 Heraklion, Greece*
[3]*ELI Attosecond Light Pulse Source, ELI-Hu Kft., Dugonics ter 13, 6720 Szeged Hungary*
(Received 18 September 2013; published 27 June 2014)

Coherent processing of quantum information and attosecond science have had so far little in common. We here show that recent data in high harmonic emission reveal a realization of a qubit and its coherent manipulation at the attosecond time scale. By observing the interference pattern created by the spatiotemporal overlap of photons emitted by two interfering electron paths we generate a photon Hadamard gate and thus erase the electron-trajectory information. This allows the measurement of the relative phase in electron-trajectory quantum superpositions which realize the qubit, opening the possibility for more elaborate schemes of coherent information processing within high-field physics.

DOI: 10.1103/PhysRevA.89.063827 PACS number(s): 42.65.Ky, 03.67.Bg, 42.50.Hz

## I. INTRODUCTION

Attosecond science is already realizing its promise as a unique quantum microscope of electron quantum dynamics at the atomic unit of time [1–5]. In recent years, the spectacular progress in attosecond pulse generation [2] has been intimately coupled with the development of new coherent light sources in the extreme ultraviolet (euv) spectral region. The physics of high harmonic generation (HHG) has been a central part of these developments. HHG results from the nonlinear interaction of intense radiation with matter. Not surprisingly, high-field and ultrafast physics have remained disconnected from another driving force of modern quantum technology, the field of quantum information processing [6]. Quantum coherent phenomena have been mostly studied in systems exhibiting long-lived quantum coherence having, until now, little relevance to ultrafast (attoscale) electron dynamics. Although electron-quantum-path interferences have been studied in HHG [7,8], the vast majority of experimental observables, like HHG spectra and cutoff laws, could be largely understood even within a classical [1,9] or at most a semiclassical model [7], without any need to resort to quantum coherence effects or the quantized-radiation formalism [10–14], the relevance of which has been debated due to the intense driving laser involved in HHG.

We here argue that the physical observables in HHG discussed in [15] can be interpreted in the context of attosecond quantum optics and related to attosecond quantum information processing. In particular, we interpret the recently observed interference of photons stemming from different electron trajectories with quantum erasure [16,17] of electron-trajectory information. Through this quantum erasure we can access the relative phase in the electron-trajectory qubit. In Sec. II we present data connecting the visibility of the photon interference pattern created through this quantum erasure with the properties of coherent superposition of electron trajectories. As a further consistency check of our analysis we unravel the connection of the electron wave-packet interference with the properties of the harmonic emission. Also, we theoretically describe our observations by introducing electron-photon ($e$-$p$) quantum coherence and entanglement and, necessarily, the quantized-radiation formulation [10–14] of HHG. Lastly, in Sec. III we reason why our measurement is dominated by the single-atom response and discuss the potential extension of this work to higher-dimensional quantum bits.

## II. RECOLLISION PROCESS AT THE QUANTUM-OPTICAL LEVEL

The process of HHG [18–22] at the single-atom level is governed by the electron quantum path interference [7,8], the properties of which, and hence the properties of the emitted harmonics, strongly depend on the intensity, $I_\ell$, of the driving laser. This determines the ponderomotive potential, $U_p$, seen by the electrons during their travel in the continuum. In the plateau spectral region there are mainly two [7] intensity-dependent electron trajectories with different path lengths, the long ($L$) and the short ($S$), that contribute to the off-axis and on-axis harmonic emission [23] with phases $\phi^L(I_\ell)$ and $\phi^S(I_\ell)$, respectively. The simultaneous presence of those trajectories is an impediment to attosecond pulse generation [24]; hence so far spatially distinguishable euv photons from *either* the $L$ *or* the $S$ trajectory were detected. This mode of detection, however, automatically eliminates the available quantum information imprinted in the quantum superpositions of $S$ and $L$ photons, which naturally arise from the Hamiltonian $e$-$p$ interaction during the HHG process. It is the spatiotemporal overlap of $S$- and $L$-trajectory photons performed in [15] and the resulting $I_\ell$-dependent interference pattern that allows measurement of the phase difference $\Delta\phi^{S,L} = \phi^S(I_\ell) - \phi^L(I_\ell)$. This is physically possible because of the coherent manipulation of the *underlying* quantum coherence of HHG photons as is explained in the following.

In Fig. 1(a) we show the experimental scheme used for the data presented here and in [15]. Instead of detecting either $S$- or $L$-trajectory HHG photons, both off-axis and on-axis HHG photons were focused at the ionization detector. In order to visualize the experimental data to be presented in the following and to substantiate the quantum information description of HHG, we calculate the euv interference pattern along the laser propagation axis ($z$ axis) for three different values of $I_\ell$, shown

*ptzallas@iesl.forth.gr

 

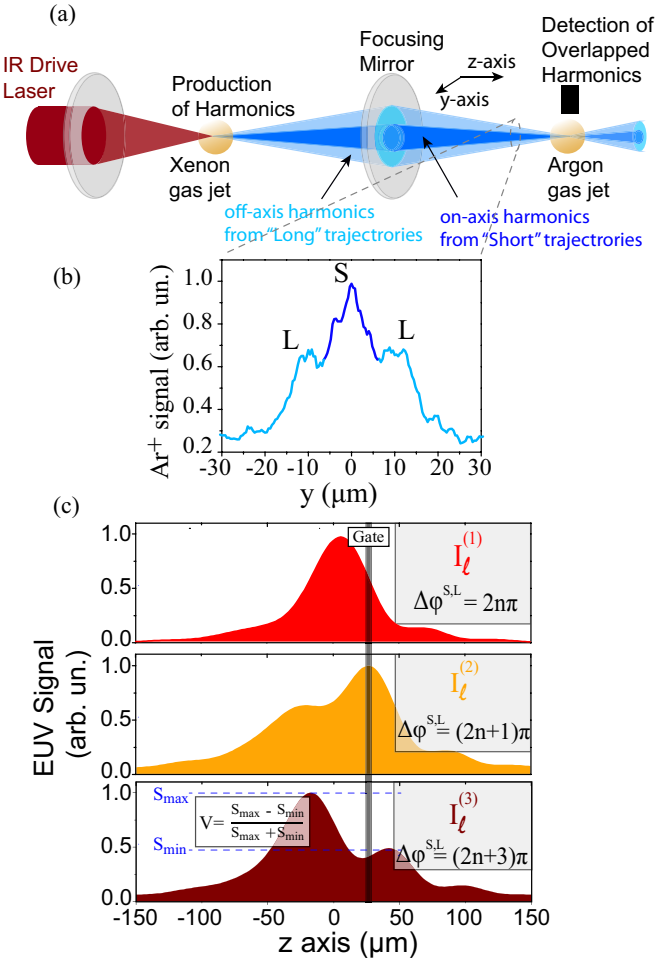


FIG. 1. (Color online) (a) Experimental scheme for realizing a HHG-photon Hadamard gate. The ir drive laser is focused on a xenon gas jet where the HHG photons are produced. On-axis (stemming from $S$ trajectories) and off-axis (stemming from $L$ trajectories) photons are then focused onto an argon gas jet, the ions of which are detected. (b) The measured euv ionization signal along the $y$ axis, depicting the on-axis and off-axis photons. The overlap of the $S$ and $L$ peaks is partly due to the projection of the actually well-separated beams on the ion detector. (c) Calculated $Ar^+$ signal, proportional to the euv intensity, as a function of distance along the $z$ axis, shown for three different values of $I_\ell$ and the corresponding phase differences $\Delta\phi^{S,L}$. The visibility of the interference pattern is limited by the out-of-plane signal in the projected focus image.

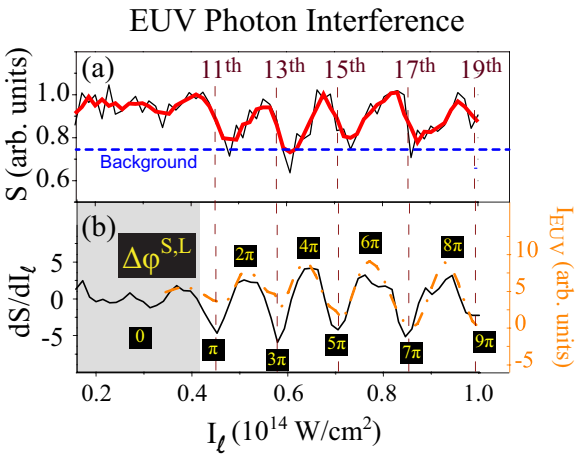


FIG. 2. (Color online) (a) Black line: Measured euv signal $S(I_\ell)$ at $z \approx 20$ $\mu$m away from focus as a function of $I_\ell$. Red line: Three-point average of signal $S(I_\ell)$ with the thickness being one standard deviation. Blue-dashed line: Background stemming from (i) the unfocused euv beam and (ii) the projected focus image [discussed in Fig. 1(c)]. Relative to this background, the visibility of the fringes is $V \approx 1$. (b) Derivative $dS/dI_\ell$. Maxima (minima) correspond to constructive (distructive) interference of euv photons with their relative phase $\Delta\phi^{S,L}$ being even (odd) multiples of $\pi$. At low intensities $I_\ell$ the harmonics are in the deep cutoff region and the two trajectories degenerate to one with a common phase; hence in the gray-shaded region $\Delta\phi^{S,L} = 0$. The orange-dashed-dotted line (right $y$ axis) is the calculated euv intensity at $z = 0$. It provides a consistency check in that $dS/dI_\ell$ reflects the euv modulation at $z = 0$. The vertical dashed lines are the measured $I_\ell$ values at which another harmonic order enters the plateau.

in Fig. 1(c). The interference maximum oscillates along the $z$ axis due the $I_\ell$ dependence of the phase difference, $\Delta\phi^{S,L}$, between $S$- and $L$-trajectory photons. The maximum visibility is obtained at 20 $\mu$m out of focus, and it is there that we place a gate to measure the euv signal modulation $S(I_\ell)$, shown in Fig. 2(a). However, we can infer the euv modulation at $z = 0$ from the derivative $dS/dI_\ell$, since the excursion of the peak in Fig. 1(c) along the $z$ axis is 40 $\mu$m. The derivative $dS/dI_\ell$ is depicted in Fig. 2(b), superimposed with the intensity of the harmonic radiation. The latter is calculated from $I(z = 0) = |E_{\rm tot}(z = 0)|^2 = \sum_q |E_q^S(I_\ell) + E_q^L(I_\ell)e^{-i\Delta\phi^{S,L}(I_\ell)}|^2$, where the sum runs through the detected harmonics $q$ ($q = 11, 13, 15$). To calculate $I(z = 0)$ we use the *independently measured* values for the $L$- and $S$-trajectory electric field amplitudes of each harmonic, $E_q^L$ and $E_q^S$, respectively, and the *measured* phase difference $\Delta\phi^{S,L}$, linearly interpolated between the minima and maxima of Fig. 2(b). We note that the minima (maxima) of the modulation shown in Fig. 2(b), which are the points of destructive (constructive) interference at the focus $z = 0$, are on par with the minima (maxima) of the total harmonic intensity. Importantly, since $U_p \propto I_\ell$, it is readily found that the beating period of the oscillations in Fig. 2(b) corresponds to a cutoff energy change by $2\hbar\omega_\ell$, i.e., $3.2U_p/\hbar\omega_\ell = 2$, where $\omega_\ell$ is the drive-laser frequency. Thus for every two ir photons removed from the drive laser another (odd) harmonic order crosses from the cutoff into the plateau region, demonstrating energy conservation at the quantized electron-photon picture.

The physical basis of our ability to measure $\Delta\phi^{S,L}$ is the access to the entangled $e$-$p$ state created by the Hamiltonian $e$-$p$ interaction. In particular, we demonstrate that the classical three-step model of HHG [9] is at the fundamental quantum-mechanical level a quantum computation, the diagram of which is shown in Fig. 3. To clearly explain the physics, we consider just one mode for the HHG photons emitted by $L$ or $S$ trajectories, call it $|1_S\rangle$ or $|1_L\rangle$, denoting a single photon in either state, while the vacuum is $|0\rangle$. The initial ($t = 0$) and final $e$-$p$ states in the HHG process are then $|\Psi_i\rangle = |\Phi_0\rangle \otimes |n_i\rangle \otimes |0\rangle$ and $|\Psi_f\rangle = |\Phi_0\rangle \otimes |n_f\rangle \otimes |1\rangle$, respectively, where $\Phi_0(\mathbf{r}) = \langle \mathbf{r}|\Phi_0\rangle$ is the ground-state electron wave function from which the electron is ionized and to which it recombines,

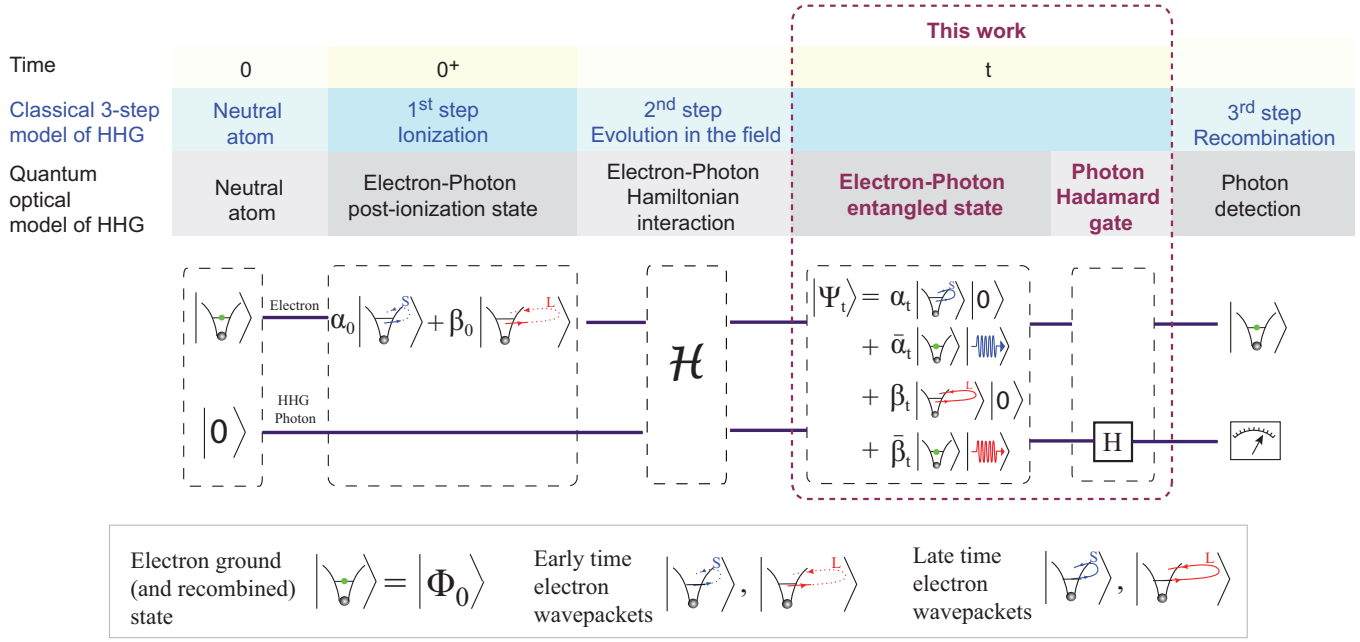


FIG. 3. (Color online) The three-step model of HHG is shown in the context of quantum information processing. The drive ir laser initiates the electronic wave function in a coherent superposition of ($L$) and ($S$) trajectories. The initial HHG photon state (for simplicity we omit the drive-laser photons) is the vacuum. Due to the Hamiltonian $e$-$p$ interaction, the $e$-$p$ state is entangled at some intermediate time smaller than about 1 fs. The Hadamard gate before the HHG photon detection allows the measurement of the relative phase of the amplitudes $\overline{\alpha}_t$ and $\overline{\beta}_t$ in the entangled state $|\Psi_t\rangle$.

$|n_i\rangle$ and $|n_f\rangle$ are the initial and final photon number states of the ir drive laser, and $|1\rangle$ is the harmonic photon produced, while $|0\rangle$ is the vacuum state. As shown in [11–13], the HHG process can be viewed as a transition from the initial state $|\Psi_i\rangle$ to intermediate quantum Volkov states $|\psi_V\rangle$, followed by the transition of the latter to the final state $|\Psi_f\rangle$, summed over all possible electron momenta $\mathbf{P}$ and photon numbers $n$ of the quantum Volkov state. However, it is known [7] that among all possible electron paths, there are two that prevail in this sum, namely, the $S$ and the $L$ trajectory. Hence just after the start of the ionization process (time $t = 0^+$), the electron and drive-laser photon state can be considered to be in a quantum superposition of quantum Volkov states that will evolve into an $S$ and an $L$ trajectory:

$$|\psi\rangle_{t=0^+} = \alpha_0 \left|\psi_V^{\mathrm{S}}\right\rangle_{t=0} + \beta_0 \left|\psi_V^{\mathrm{L}}\right\rangle_{t=0}. \tag{1}$$

The amplitudes $\alpha_0$ and $\beta_0$ depend on experimental parameters such as the laser focus position with respect to the gas jet (and as is shown next, in our case it is $|\alpha_0| \approx |\beta_0|$). The total $e$-$p$ state will then be

$$|\Psi_{t=0^+}\rangle = |\psi\rangle_{t=0^+} \otimes |0\rangle, \tag{2}$$

where the HHG photon state is the vacuum. The $e$-$p$ Hamiltonian interaction will time-evolve $|\Psi_{t=0^+}\rangle$ to the entangled state

$$|\Psi_t\rangle = \alpha_t \left|\psi_V^S\right\rangle_t \otimes |0\rangle + \beta_t \left|\psi_V^L\right\rangle_t \otimes |0\rangle + \overline{\alpha}_t |\Phi_0\rangle \otimes |n_f\rangle \otimes |1_S\rangle + \overline{\beta}_t |\Phi_0\rangle \otimes |n_f\rangle \otimes |1_L\rangle, \tag{3}$$

which is a coherent superposition of four terms, describing the amplitude for an $S$- or an $L$-trajectory electron to have (third and fourth terms) or not to have (first and second terms) recombined at time $t$. Clearly, the amplitudes $\overline{\alpha}_t$ and $\overline{\beta}_t$ (obviously $\overline{\alpha}_0 = \overline{\beta}_0 = 0$) determine the probability for an $S$ or an $L$ photon to be emitted at time $t$. Their relative phase at time $t$, $\Delta\phi^{S,L}$, reflects, besides the initial relative phase of $\alpha_0$ and $\beta_0$, the different phase acquired by the electron along the $S$ or the $L$ trajectory. Defining $r = |\overline{\beta}_t/\overline{\alpha}_t|$, the part of $|\Psi_t\rangle$ containing one HHG photon will be proportional to

$$|\Psi_t'\rangle = |\Phi_0\rangle \otimes |n_f\rangle \otimes \left(|1_S\rangle + re^{-i\Delta\phi^{S,L}}|1_L\rangle\right). \tag{4}$$

It is clear that if we were to detect *either* on-axis *or* off-axis photons, i.e., if were we to measure the HHG photon in the $\{|1_S\rangle, |1_L\rangle\}$ basis, the phase $\Delta\phi^{S,L}$ would not be observable. However, now that we apply a Hadamard gate [25] before the photon detection, i.e., overlap the on- and off-axis photons and let them interfere, we measure in a different basis spanned by the photon states $|1_\pm\rangle = (|1_S\rangle \pm |1_L\rangle)/\sqrt{2}$, where we assumed for simplicity that our interferometer works like a 50:50 beam splitter. In terms of $|1_\pm\rangle$ we can write

$$|\Psi_t'\rangle = \frac{1}{\sqrt{2}}|\Phi_0\rangle \otimes |n_f\rangle \otimes \left[\left(1 + re^{-i\Delta\phi^{S,L}}\right)|1_+\rangle + \left(1 - re^{-i\Delta\phi^{S,L}}\right)|1_-\rangle\right]. \tag{5}$$

It is now clear that detecting the photon in the $|1_\pm\rangle$ basis leads to an $I_\ell$-dependent interference pattern of the form $(1 + r^2) + 2r\cos\Delta\phi^{S,L}$. Therefore the phase of the interference pattern is the phase difference $\Delta\phi^{S,L}$, while its visibility $2r/(1 + r^2)$ encodes the factor $r$ embodying information about the initial quantum superposition of electron trajectories. The visibility inferred from the interference pattern of Fig. 2(a) is $V \approx 1$; hence $r \approx 1$. This is consistent with the photon statistics of $S$ or $L$ photons. Indeed, from Eq. (4) it follows that, if we separately

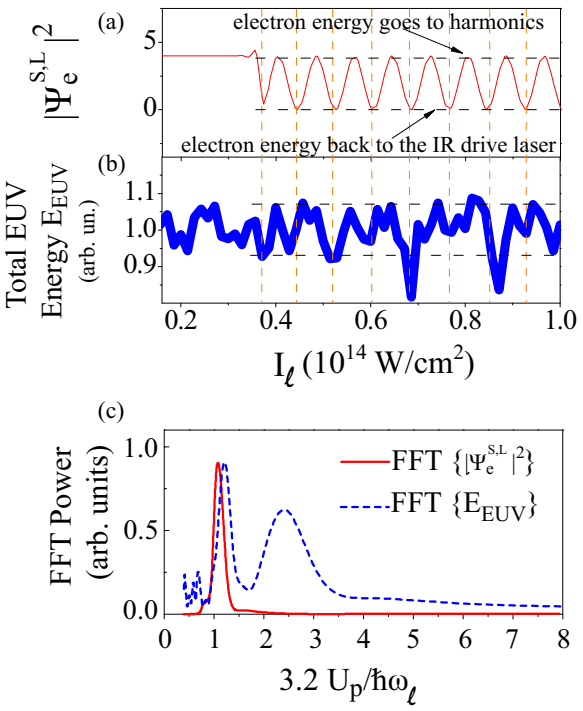


FIG. 4. (Color online) (a) Calculated probability density of two interfering plane waves with $I_\ell$-dependent phases. (b) Measured volume-integrated harmonic yield, oscillating on par with the probability density. The modulation sits on top of an $I_\ell$-increasing background which has been subtracted away. The maxima (minima) of the beatings (horizontal dashed lines) correspond to the electron energy going to the harmonics (returning to the driving ir field). The line thickness is the measurement error. The oscillations observed in the harmonic yield are in fair agreement with those calculated by using a simple electron wave-packet interference model. This is depicted by the vertical dashed lines which show the matching between the calculated and measured oscillation minima. (c) FFT spectrum (with the $x$ axis being proportional to the period) of modulations (a) and (b) plotted with red and blue dashed lines, respectively. Both have a component corresponding to $\hbar\omega_\ell$, while the modulation (b) has a second component corresponding to $2\hbar\omega_\ell$, due to the generated harmonics entering the plateau.

detect either $S$ or $L$ photons, their relative rate will be $r^2$. We measured this relative rate and found that $r^2 \approx 1.3 \pm 0.2$, consistent with the value of $r$ obtained from the visibility of the $I_\ell$-interference pattern.

To further elaborate on how the electron-trajectory qubit is imprinted on the HHG photon qubit we plot in Fig. 4(a) the electron wave-packet probability density corresponding to a superposition of the form (1). Simulating these wave packets with simple plane waves moving just along the polarization of the drive laser ($x$ axis), the probability density at the nucleus (where recombination takes place) will be $|\Psi_e^{S,L}|^2 = |\alpha e^{-ik_x x_S(I_\ell)} + \beta e^{-ik_x x_L(I_\ell)}|^2$, where $x_S(I_\ell)$ and $x_L(I_\ell)$ are the $I_\ell$-dependent path lengths of the $S$ and the $L$ trajectory, respectively. Since $r \approx 1$, it is $|\Psi_e^{S,L}|^2 \propto 1 + \cos(k_x \Delta x^{S,L})$, where $\Delta x^{S,L}(I_\ell) = x_S - x_L$. It can be shown [15] that $k_x \Delta x^{S,L}$ is a linear function of the intensity $I_\ell$, and it is through this dependence that the modulation of Fig. 4(a) is produced. The probability is seen to oscillate with a period corresponding to a cutoff energy change by $\hbar\omega_\ell$, i.e., $3.2Up_p/\hbar\omega_\ell = 1$, as depicted in the FFT spectrum of Fig. 4(c). This result further supports the quantized-radiation picture of HHG. Indeed, for yet another drive-laser photon absorbed, an additional momentum $\hbar k_\ell$ is transferred to the electrons, and the $S$-$L$ path length difference $\Delta x^{S,L}$ changes by a de Broglie wavelength $\lambda_e$, leading to a phase difference $\Delta\phi^{S,L} = 2\pi$. Thus, the modulation's maxima (minima) correspond to the case when the $S$ and $L$ trajectories interfere constructively (destructively) and the electron's kinetic energy goes to the harmonics (back to the drive-laser field). This is corroborated by the *measured* harmonic yield (volume-integrated harmonic intensity) shown in Fig. 4(b). Its power spectrum [Fig. 4(c)] also exhibits a peak at $3.2U_p/\hbar\omega_\ell = 1$. Put another way, adding another photon to the drive-laser field, and since even harmonics are ruled out by symmetry, the extra energy either goes to increasing the production rate of odd harmonics or goes back to the field. Incidentally, we also observe a modulation component at $3.2U_p/\hbar\omega_\ell = 2$, reflecting an additional harmonic order entering the plateau region. This is in agreement with the selection rule for the generation of odd-order harmonics and consistent with the harmonic cutoff positions discussed in Fig. 2.

## III. DISCUSSION

Lastly, we have to make two clarifying points regarding (a) the single-atom response versus medium effects and (b) the possible presence of multiple electron trajectories.

(a) Although the produced euv radiation stems from the coherent contribution of the medium's atoms, our measurement is dominated by the single-atom response. Indeed, the outgoing euv photon ($q$th harmonic) wave vector is $\mathbf{k}_q = q\mathbf{k}_\ell + \Delta\mathbf{k}_g + \Delta\mathbf{k}_d + \nabla\phi_q^{S,L}(I_\ell)$, where $\mathbf{k}_\ell$ is the wave vector of the fundamental. The Gouy phase shift, $\Delta\mathbf{k}_g$, and the dispersion mismatch, $\Delta\mathbf{k}_d$, account for the macroscopic propagation effects, while $\nabla\phi_q^{S,L}(I_\ell)$ represents the single-atom response. The reasons we access the single-atom level are (i) the term $\Delta\mathbf{k}_d$ is absent since $\Delta\phi^{S,L}$ is obtained from the same harmonic frequency, (ii) the term $\Delta\mathbf{k}_g$ and the intensity variation of the driving laser along its propagation in the medium are negligible since the confocal parameter of the ir beam is much larger than the medium length, and (iii) we spatially resolve interference maxima and minima resulting from the overlap of the *same* frequency of $S$- and $L$-trajectory harmonics. Thus, any intensity variation of the driving field is inconsequential.

(b) Although the existence of additional electron trajectories as predicted in the case of neon and argon cannot be excluded, the present findings are consistent with the dominance of two trajectories [26]. This is because from the linear dependence of $\phi_q^{S,L}(I_\ell)$ on $I_\ell$ and the data of Fig. 2 it is found that for $q = 11$–$15$ the proportionality constant $\alpha_q^{\mathrm{L}} - \alpha_q^{\mathrm{S}} \approx 40 \times 10^{-14}$ rad cm$^2$/W, which is in agreement with previous experimental findings [27] and the theoretical predictions for the dominance of the two shortest electron trajectories [7,26,28]. Regarding the connection we make with quantum information processing, the case with more than two trajectories would be interesting in its own right

because physically it represents not a qubit but a qudit, i.e., a higher-dimensional quantum bit.

## IV. CONCLUSIONS

In summary, we have experimentally demonstrated the quantum-optical nature of the recollision process in HHG, interpreting our experimental results in the context of quantum information. We have interpreted our HHG photon interference measurement in the context of a Hadamard gate at the attosecond time scale which coherently manipulates the HHG photon. Thus we reveal the phase in the electron trajectory qubit that gives rise to the HHG photon at the recombination. Although we did not directly measure the electron-photon entanglement prior to recombination, its existence is a necessary condition for the observed interference pattern. Finally, although this work is obviously far from coherently manipulating multiple qubits, we demonstrate that concepts and techniques from quantum optics and quantum information processing are physically and experimentally related to high-field physics.

## ACKNOWLEDGMENTS

This work was supported by Laserlab Europe, the Greek funding program NSRF, and the European Union's Seventh Framework Programme FP7-REGPOT-2012-2013-1 under Grant No. 316165. We also acknowledge B. Bergues, H. Schröder, and L. Veisz from the Max Planck Institut für Quantenoptik for sharing the ion microscope through the DAAD-IKYDA program.

[1] P. B. Corkum and F. Krausz, Nat. Phys. **3**, 381 (2007).
[2] F. Krausz and M. Ivanov, Rev. Mod. Phys. **81**, 163 (2009).
[3] J. M. Dahlström, A. L'Huillier, and A. Maquet, J. Phys. B **45**, 183001 (2012).
[4] P. Tzallas *et al.*, Nat. Phys. **7**, 781 (2011).
[5] E. Goulielmakis *et al.*, Nature (London) **466**, 739 (2010).
[6] D. J. Wineland, Rev. Mod. Phys. **85**, 1103 (2013).
[7] M. Lewenstein, Ph. Balcou, M. Y. Ivanov, A. L'Huillier, and P. B. Corkum, Phys. Rev. A **49**, 2117 (1994).
[8] A. Zaïr *et al.*, Phys. Rev. Lett. **100**, 143902 (2008).
[9] P. B. Corkum, Phys. Rev. Lett. **71**, 1994 (1993).
[10] D. S. Guo and G. W. F. Drake, J. Phys. A: Math. Gen. **25**, 3383 (1992); **25**, 5377 (1992).
[11] J. Gao, F. Shen, and J. G. Eden, Phys. Rev. Lett. **81**, 1833 (1998); Phys. Rev. A **61**, 043812 (2000).
[12] J. Gao, D. S. Guo, and Y. S. Wu, Phys. Rev. A **61**, 043406 (2000).
[13] L. Gao, X. Li, P. Fu, R. R. Freeman, and D. S. Guo, Phys. Rev. A **61**, 063407 (2000).
[14] S. Varró, Phys. Scr. T **140**, 014038 (2010).
[15] G. Kolliopoulos *et al.* (unpublished), arXiv:1307.3859.
[16] T. J. Herzog, P. G. Kwiat, H. Weinfurter, and A. Zeilinger, Phys. Rev. Lett. **75**, 3034 (1995).
[17] Y. H. Kim, R. Yu, S. P. Kulik, Y. Shih, and M. O. Scully, Phys. Rev. Lett. **84**, 1 (2000).
[18] Y. Mairesse *et al.*, Science **302**, 1540 (2003).
[19] X. Zhang, A. L. Lytle, O. Cohen, M. M. Murnane, and H. C. Kapteyn, New J. Phys. **10**, 025021 (2008).
[20] L. Brugnera, D. J. Hoffmann, T. Siegel, F. Frank, A. Zaïr, J. W.G. Tisch, and J. P. Marangos, Phys. Rev. Lett. **107**, 153902 (2011).
[21] D. Shafir *et al.*, Nature (London) **485**, 343 (2012).
[22] O. Raz *et al.*, Nat. Photonics **6**, 170 (2012).
[23] M. Bellini, C. Lyngå, A. Tozzi, M. B. Gaarde, T. W. Hansch, A. L'Huillier, and C.-G. Wahlström, Phys. Rev. Lett. **81**, 297 (1998).
[24] M. B. Gaarde and K. J. Schafer, Phys. Rev. Lett. **89**, 213901 (2002).
[25] J. M. Raimond, M. Brune, and S. Haroche, Rev. Mod. Phys. **73**, 565 (2001).
[26] M. B. Gaarde, J. L. Tate, and K. J. Schafer, J. Phys. B **41**, 132001 (2008).
[27] C. M. Heyl, J. Güdde, U. Höfer, and A. L'Huillier, Phys. Rev. Lett. **107**, 033903 (2011).
[28] K. Varju *et al.*, J. Mod. Opt. **52**, 379 (2005).